**Supplementary Information**

# Over 8% efficient $CsSnI_3$-based mesoporous perovskite solar cells enabled by two-step thermal annealing and surface cationic coordination dual treatment

Huaxia Ban, [a] Takahito Nakajima, [b] Zhirong Liu, [a] Haixuan Yu, [a] Qiang Sun, [a] Letian Dai, [a] Yan Shen, [a] Xiao-Li Zhang, [c] Jun Zhu, [d] Peter Chen [e] and Mingkui Wang [a, *]

[a] Wuhan National Laboratory for Optoelectronics, Huazhong University of Science and Technology, 1037 Luoyu Road, Wuhan 430074, Hubei, P. R. China

[b] RIKEN Center for Computational Science, 7-1-26 Minatojima-minami-machi, Chuo-ku, Kobe, Hyogo, 650-0047 Japan

[c] State Centre for International Cooperation on Designer Low-Carbon & Environmental Materials, School of Materials Science and Engineering, Zhengzhou University, 450001, P. R. China.

[d] Special Display and Imaging Technology Innovation Center of Anhui Province, State Key Lab of Advanced Display Technology, Key Lab of Advance Functional Materials and Devices of Anhui Province, Academy of Opto-Electric Technology, Hefei University of Technology, 193 Tunxi Road, Hefei, 230009, P. R. China.

[e] Department of Photonics, National Cheng Kung University, Tainan, 701, ROC

*** Corresponding author, E-mail: mingkui.wang@mail.hust.edu.cn (M. Wang)**

## Experimental Section

***Materials:*** CsI (99.99%, Sigma Aldrich), $SnI_2$ (99.99%, Sigma Aldrich), 1-(4-Carboxyphenyl)-2-thiourea (97%, Alfa Aesar), N, N-Dimethylformamide (DMF, Anhydrous 99.8%, Sigma Aldrich), and dimethyl sulfoxide (DMSO, Anhydrous ≥ 99.5%, Sigma Aldrich) were used as received without further purification.

***All-inorganic mesoscopic framework fabrication:*** All-inorganic mesoscopic framework was fabricated on fluorine doped tin oxide (FTO) coated glass used as transparent electrode and substrate, respectively. The etched FTO glass was sequentially ultrasonically cleaned with detergent, water, deionized water, and ethanol. Then, FTO was treated by UV ozone for 30 min. Subsequently, a 50 nm thick compact $TiO_2$ layer was deposited on the cleaned FTO substrate by spray pyrolysis deposition with titanium isopropoxide (trance metals basis, Aldrich) ethyl alcohol solution at 450°C, keeping at this temperature for 30 min. After cooled to room temperature, a 400 nm-thick mesoporous $TiO_2$ nanocrystal film (DSL 30NR-T, Dyesol, Australia, diluted with terpinol, 1/3.5 mass ratio), a 450 nm-thick $Al_2O_3$ insulating layer (20 nm $\gamma$-$Al_2O_3$ nanoparticles, Aladdin), an 800 nm-thick NiO layer (30 nm sized nanoparticles, Inframat) were sequentially deposited with screen printing method onto FTO. Following heating the paste in the air flow with a procedure of 112 °C for 5 min, 175 °C for 5 min, 350 °C for 10 min, 400 °C for 15 min, and 500 °C for 30 min. Then, the carbon paste was blade coated on the dry film (on the top of the NiO layer) as the top electrode and sintered in the air at 400 °C for 30 min. The thickness of the top electrode is 10 μm. The thickness of each layer was measured by profile-system (DEKTAK, VEECCO, Bruker).

***PSC devices fabrication:*** CsI, $SnI_2$ and 1-(4-Carboxyphenyl)-2-thiourea with a molar ratio of 1: 1.1: (0.05, 0.1, 0.15) were dissolved in mixed solvent of DMF and DMSO (1:4 in volume ratio) to obtain 0.8 M/L solution. After preparing the precursor solution, stir it on a magnetic stirrer for 4 hours, and use it directly after filtering the solution. A 2.5μL solution was dropped on the prepared all-inorganic FTO/c-$TiO_2$/m-$TiO_2$/$Al_2O_3$/NiO/carbon mesoporous framework, and let the device stand for 5 min to allow the solution to fully infiltrate the mesoporous structure, and then performed annealing treatment (40 °C for 5 min, 70 °C for 5 min) to finish the device fabrication. All the fabrication steps were conducted in a $N_2$-filled glove box.

***$CsSnI_3$ films fabrication:*** The films were fabricated on glasses in a $N_2$-filled glove box. The substrates were sequentially ultrasonically cleaned with detergent, water, deionized water, and ethanol. Then, the substrates were treated by UV ozone for 30 min. The prepared precursor solution was deposited on the substrate through the one-step spin coating process (30 s at 2000 rpm) and let the wet film stand for 3 min. Finally, the substrate was annealed at 40 °C for 5 min and 70 °C for 5 min to finish the $CsSnI_3$ film fabrication.

***Characterization:*** X-ray diffraction (XRD) experiments were conducted using a Philips X-ray diffractometer with Cu Kα radiation to measure the crystal structure. The film light absorption was measured with a PE950 spectrophotometer at room temperature. The film morphology was obtained with a field-emission scanning electron microscope (FEI Nova Nano SEM 450). The steady-state photoluminescence (PL) spectrum was measured by a fluorescence spectrophotometer (LabRAM HR800). FT-IR spectra were measured by using a FT-IR spectrometer with a diamond ATR (Frontier Optica, PerkinElmer). The liquid-state NMR was performed by VNMRS 600. X-ray photoelectron spectrometer (XPS) measurements were conducted on an AXIS SUPRA system (Kratos Analytical Ltd.). Time-resolved photoluminescence decays (TRPL) were measured by Delta Flex Fluorescence Lifetime System (Horiba Scientific Com., Japan). The photocurrent density-voltage (*J-V*) characteristics of the devices were obtained by applying external potential bias to the devices and measuring the generated photocurrent with a Keithley model 2400 digital source meter. A xenon light source solar simulator (450 W, Oriel, model 9119) with AM 1.5G filter (Oriel, model 91192) was used to give an irradiance of 100 mW $cm^{-2}$ at the surface of solar cells. All devices were measured using a metallic mask with an aperture area of 0.198 $cm^2$. A similar data acquisition system was used to control the incident photon-to-current conversion efficiency (EQE) measurement. A white-light bias (10% sunlight intensity) was applied onto the sample during the EQE measurements with the alternating current (AC) model (130 Hz). The photovoltage/photocurrent transient decay measurements were carried out to obtain the recombination/transport lifetime of solar cell devices (Hua Ming, model III). A white-light bias on the device sample was generated from an array of diodes. A pulsed green laser was used as the perturbation source, with a pulse width of 10 ns and a repetition frequency of 10 Hz. Transients were measured at different white light intensities via tuning the voltage applied to the bias diodes. The voltage/current output was recorded on an oscilloscope directly connected with the cells.

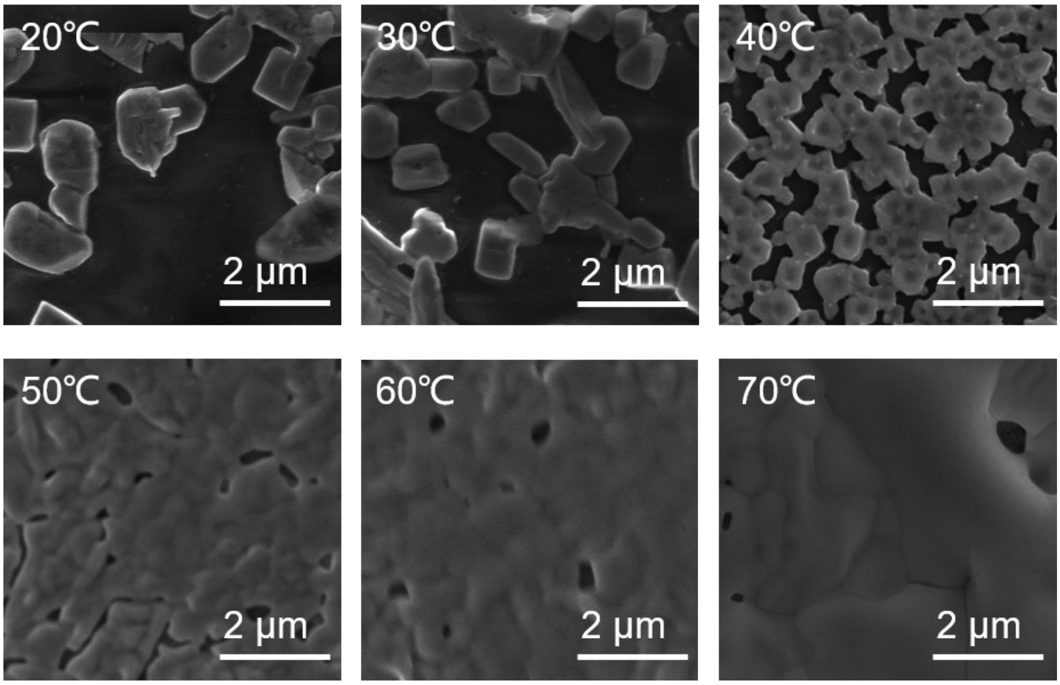


**Figure S1.** The surface SEM images of $CsSnI_3$ thin films based on different thermal annealing temperatures (20℃, 30℃, 40℃, 50℃, 60℃, 70℃) within the same annealing time. The scale bar is 2 μm.

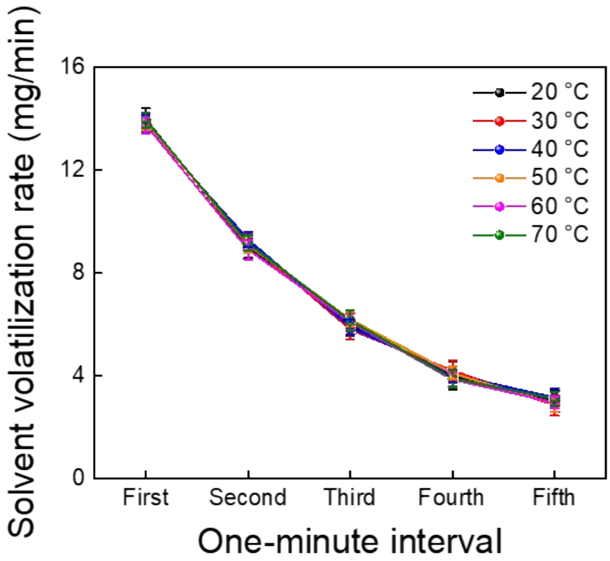


**Figure S2.** The calculated solvent volatilization rate of the samples which has reached the supersaturation concentration after annealing at different temperatures (20 °C, 30 °C, 40 °C, 50 °C, 60 °C, 70 °C) at one-minute intervals.

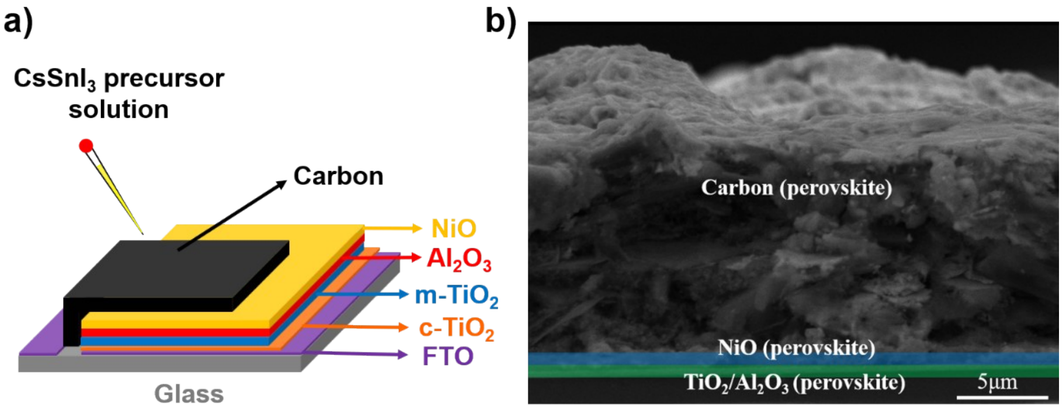


**Figure S3.** a) Schematic representation of the $TiO_2/Al_2O_3$/NiO/carbon ($CsSnI_3$) based device. b) Configuration of the $TiO_2/Al_2O_3$/NiO/carbon ($CsSnI_3$) device structure from cross section SEM image.

Each layer has been selected with its own purpose in this device structure. $TiO_2$ layer has been widely used as the ETL because of its high temperature resistance and efficient electron extraction capability. The $Al_2O_3$ layer is applied between the mesoporous $TiO_2$ (n-type) and NiO (p-type) layers to prevent the direct contact between these two semiconductors and to realize a metal oxide framework configuration. The NiO layer can accelerate the hole extraction from perovskite material. The carbon counter electrode can greatly reduce the cost of precious metal electrode and be more conducive to commercialization.[1]

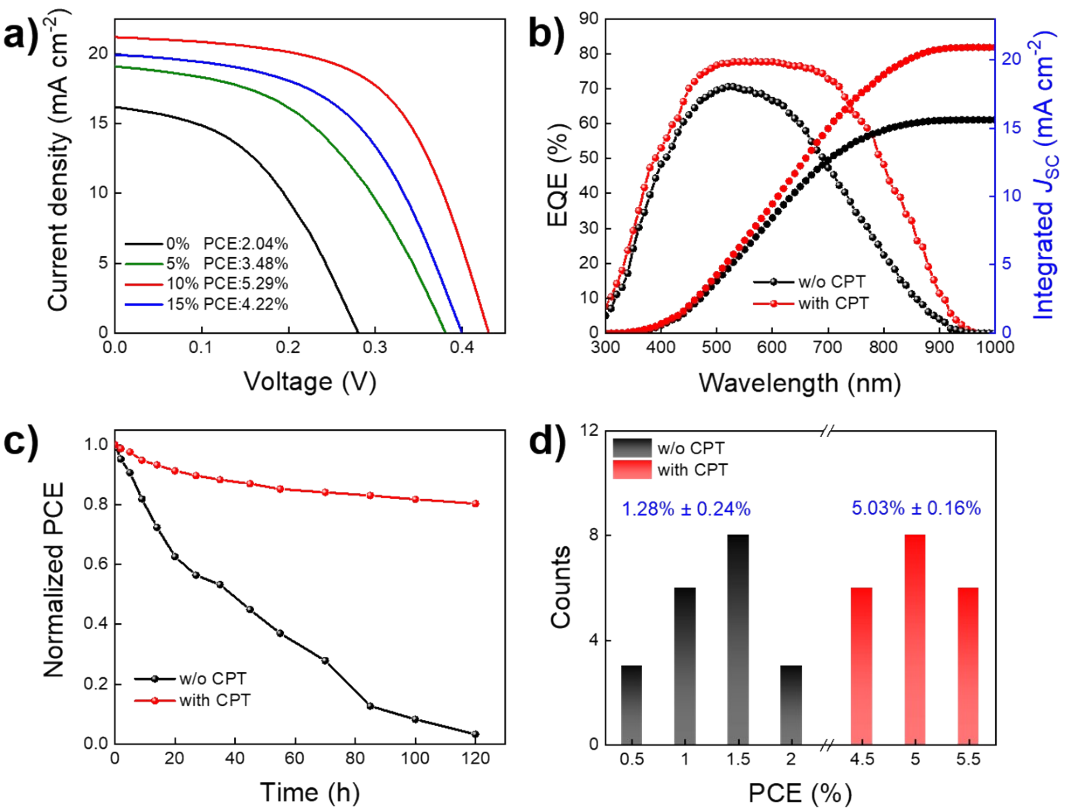


**Figure S4.** a) *J-V* curves for the best-performing $CsSnI_3$ perovskite solar cells with the addition of different concentrations of CPT (with 0, 5, 10 and 15 mol% CPT). b) EQE spectrum and the integrated current density curve of the $CsSnI_3$ perovskite solar cells without and with CPT treated. c) The normalized PCE evolution of encapsulated PSCs stored in air environment without and with CPT addition. d) PCE histograms obtained from 20 individual pristine $CsSnI_3$ perovskite solar cells and 20 individual CPT treated $CsSnI_3$ perovskite solar cells.

Figure S4b presents the external quantum efficiency (EQE) measurement of the $CsSnI_3$ solar cells without and with CPT addition. The EQE value of CPT treated $CsSnI_3$ device shows enhancement compared to that of the pristine device within the whole absorption range, resulting in the increase of integrated current density from 15.6 to 20.9 mA cm$^{-2}$. It is also worth noting that the EQE curve of the CPT treated device exhibits a significant increased intensity especially at the long wavelength range, which may be originated from the suppression of nonradiative recombination, enabling the excited charge carriers in the long wavelength to be extracted effectively by carrier extraction layers. In Figure S4c, the PCE of encapsulated pristine $CsSnI_3$ solar cell almost disappeared after 120 h storage in air environment (humidity: 60%, temperature: 25°C). The efficiency decay might be attributed to the $Sn^{2+}$ oxidation induced by air or other variables. Encouragingly, the stability is improved dramatically for the CPT treated $CsSnI_3$ solar cell, which maintained over 80% initial efficiency after aging for 120 h in the same condition, manifesting the $Sn^{2+}$ oxidation has been suppressed effectively with the aid of CPT. Finally, we made a statistic of the PCE of 20 individual reference $CsSnI_3$ solar cells and 20 individual CPT-$CsSnI_3$ solar cells. As we can see in Figure S4d, the samples with CPT treated display a narrow PCE distribution with an average of 5.03% which is higher than 1.28% of pristine PSCs, indicating the high reproducibility with CPT addition. These photovoltaic and stability characterizations clearly demonstrate that the addition of CPT is more helpful to protect $Sn^{2+}$ from oxidation and inhibit the trap-assisted nonradiative recombination through the coordination interaction between CPT and undercoordinated $Sn^{2+}$ on the surface.

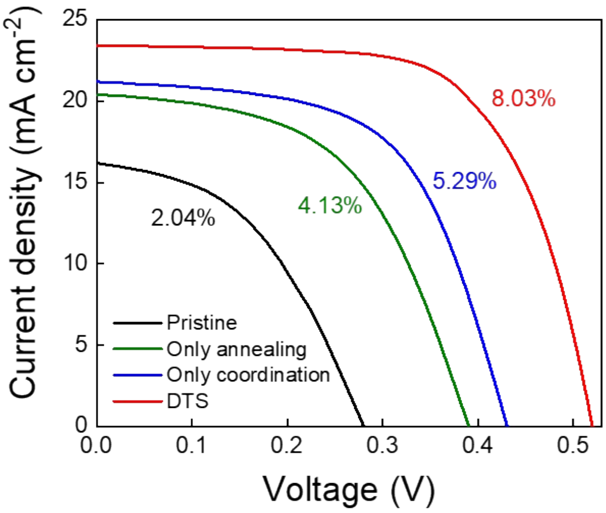


**Figure S5.** Typical *J*-*V* curves for the best-performing pristine, only two-step temperature annealing treated, only surface cationic coordination modified and DTS-treated $CsSnI_3$ perovskite solar cells under AM 1.5G one sun illumination.

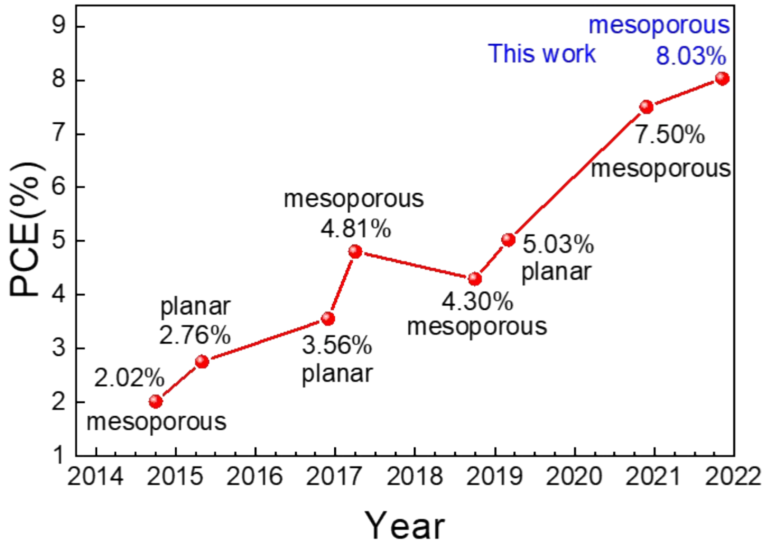


**Figure S6.** The efficiency progress of $CsSnI_3$-based perovskite solar cells over recent years. (2.02%,[2] 2.76%,[3] 3.56%,[4] 4.81%,[5] 4.30%,[6] 5.03%,[7] 7.50%.[8])

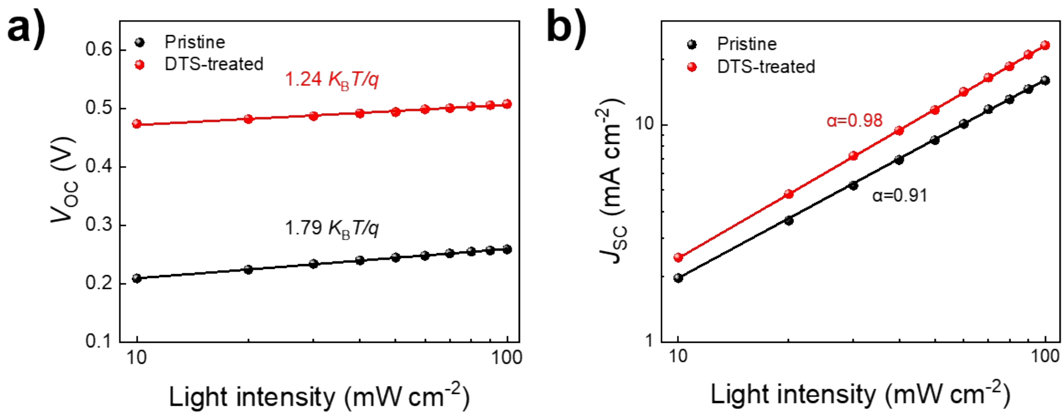


**Figure S7.** Light intensity dependence of a) open circuit voltage ($V_{OC}$) and b) short circuit current density ($J_{SC}$) for the pristine and DTS-treated $CsSnI_3$ perovskite solar cells.

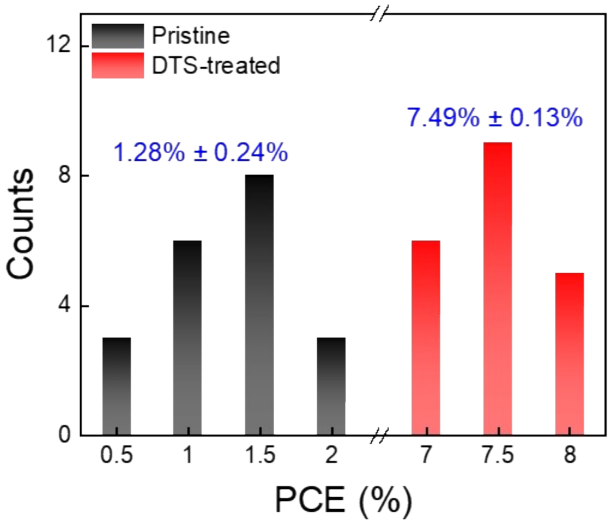


**Figure S8.** Power conversion efficiency (PCE) histograms obtained from 20 individual perovskite solar cells without and with DTS-treated.

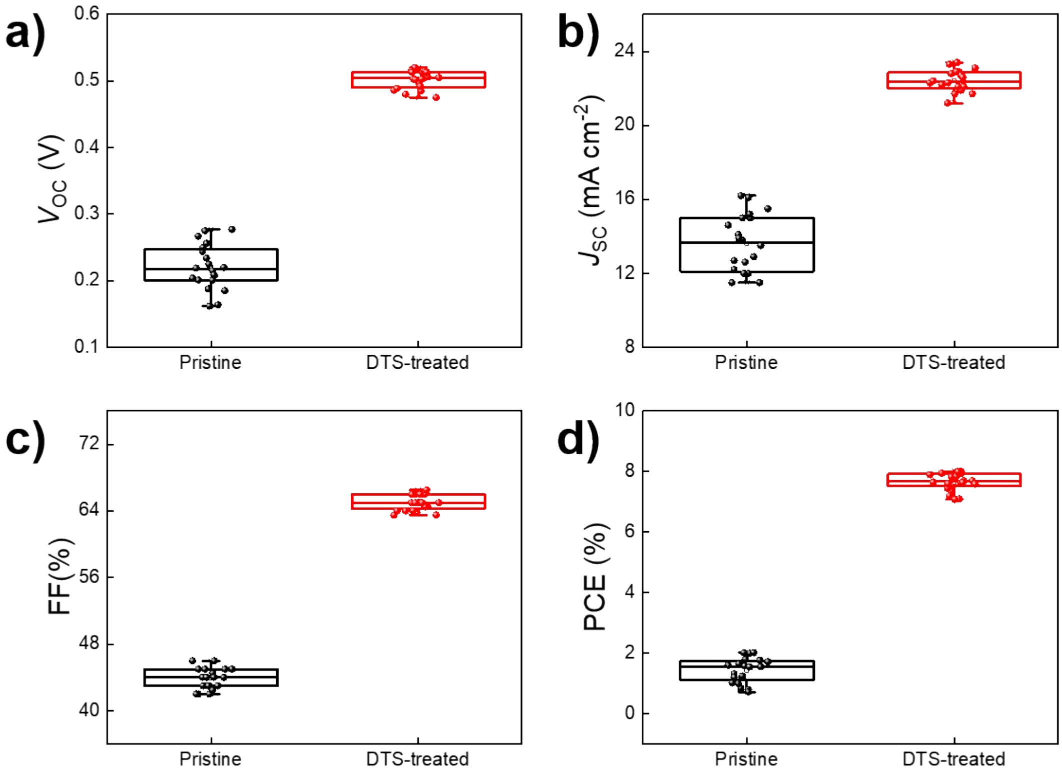


**Figure S9.** Device photovoltaic parameters of 20 individual perovskite solar cells without and with DTS-treated; a) $V_{OC}$, b) $J_{SC}$, c) FF, and d) PCE.

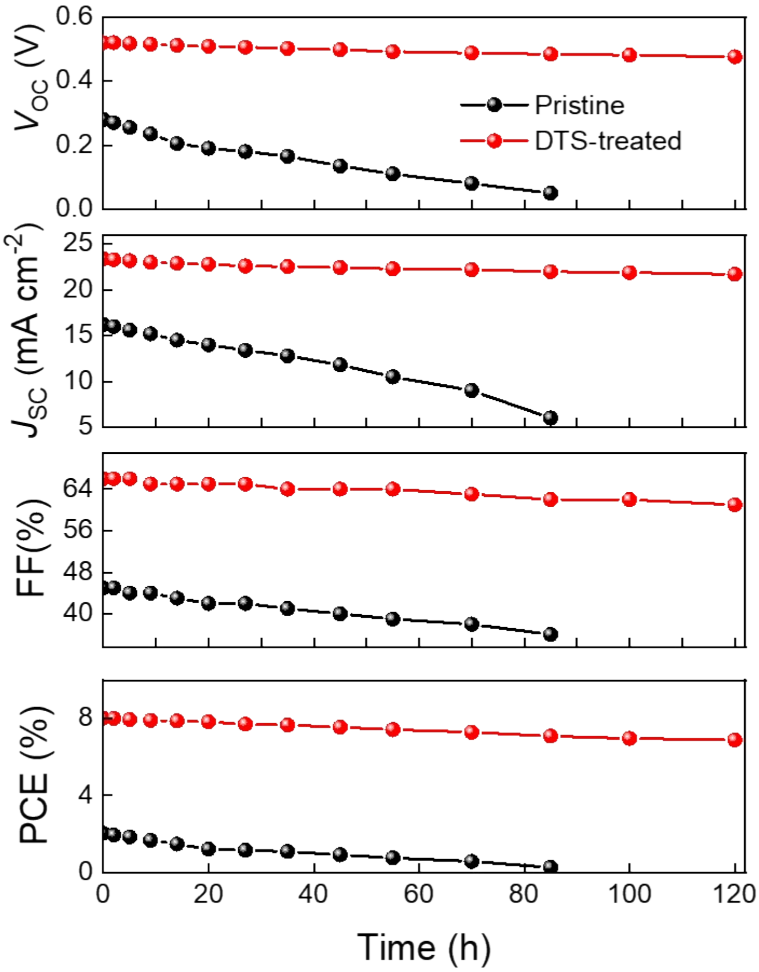


**Figure S10.** Evolution of $V_{OC}$, $J_{SC}$, FF, and PCE for the encapsulated devices without and with DTS-treated under ambient-air condition.

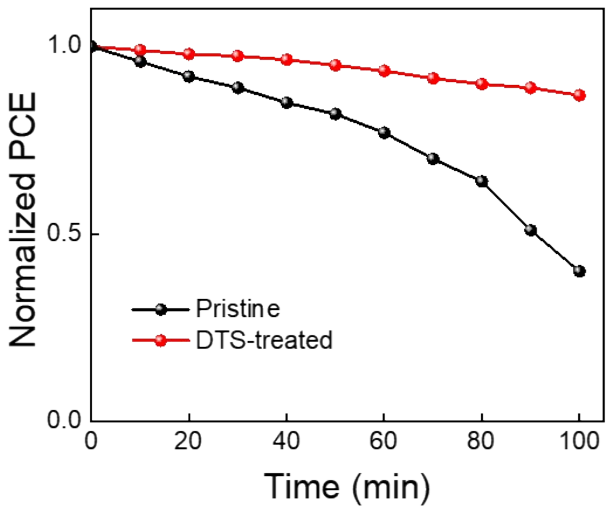


**Figure S11.** Light soaking test for the encapsulated devices without and with DTS-treated under continuous light illumination (100 mW $cm^{-2}$) in air.

**Table S1.** Detailed summary of the parameters fitted from the TRPL spectra.

| Sample | $A_1$(%) | $\tau_1$ (ns) | $A_2$(%) | $\tau_2$ (ns) | $\tau_{avg}$ (ns) |
|---|---|---|---|---|---|
| **$CsSnI_3$** | 70.3 | 4.5 | 29.7 | 18.1 | 8.5 |
| **$CsSnI_3$-CPT** | 51.8 | 10.6 | 48.2 | 27.5 | 18.8 |

**Table S2.** The photovoltaic parameters of the best-performing PSCs upon different addition ratios of CPT.

| CPT ratio | $V_{OC}$ (V) | $J_{SC}$ (mA cm$^{-2}$) | FF (%) | PCE (%) |
|---|---|---|---|---|
| **0 mol%** | 0.28 | 16.2 | 45 | 2.04 |
| **5 mol%** | 0.38 | 19.1 | 48 | 3.48 |
| **10 mol%** | 0.43 | 21.2 | 58 | 5.29 |
| **15 mol%** | 0.40 | 19.9 | 53 | 4.22 |

**Table S3.** Detailed photovoltaic parameters of PSCs without and with DTS-treated under different scan directions.

| | | $V_{OC}$ (V) | $J_{SC}$ (mA cm$^{-2}$) | FF (%) | PCE (%) |
|---|---|---|---|---|---|
| **pristine-RS[a]** | average | 0.240 ± 0.04 | 15.8 ± 0.39 | 42 ± 2.7 | 1.59 ± 0.36 |
| | champion | 0.280 | 16.2 | 45 | 2.04 |
| **pristine-FS** | average | 0.190 ± 0.05 | 15.1 ± 0.68 | 43 ± 3.1 | 1.23 ± 0.51 |
| | champion | 0.240 | 15.8 | 46 | 1.74 |
| **DTS-RS** | average | 0.510 ± 0.02 | 23.1 ± 0.32 | 65 ± 1.1 | 7.78 ± 0.24 |
| | champion | 0.520 | 23.4 | 66 | 8.03 |
| **DTS-FS** | average | 0.500 ± 0.02 | 23.0 ± 0.35 | 64 ± 2.2 | 7.51 ± 0.37 |
| | champion | 0.513 | 23.3 | 66 | 7.89 |

[a)] (RS: reverse scan; FS: forward scan)

**Table S4.** Photovoltaic performance and device structure of $CsSnI_3$ perovskite solar cells.

| Perovskite | Device structure | $V_{OC}$ (V) | $J_{SC}$ (mA cm$^{-2}$) | FF (%) | PCE (%) |
|---|---|---|---|---|---|
| **$CsSnI_3$**[2] | FTO/compact $TiO_2$/mesoporous $TiO_2$/$CsSnI_3$/m-MTDATA/Au | 0.240 | 22.70 | 37.0 | 2.02 |
| **$CsSnI_3$**[3] | ITO/CuI/$CsSnI_3$/Fullerene/BCP/Al | 0.430 | 12.30 | 39.5 | 2.76 |
| **$CsSnI_3$**[4] | ITO/$CsSnI_3$/$PC_{61}BM$/BCP/Al | 0.510 | 10.12 | 69.0 | 3.56 |
| **$CsSnI_3$**[5] | FTO/compact $TiO_2$/mesoporous $TiO_2$/$CsSnI_3$/PTAA/Au | 0.382 | 25.71 | 49.05 | 4.81 |
| **$CsSnI_3$**[6] | FTO/mesoporous $TiO_2$/ $CsSnI_3$/PTAA/Au | 0.440 | 18.50 | 52.9 | 4.30 |
| **$CsSnI_3$**[7] | ITO/PEDOT:PSS/$CsSnI_3$/PCBM/Ag | 0.420 | 23.79 | 50.3 | 5.03 |
| **$CsSnI_3$**[8] | FTO/compact $TiO_2$/mesoporous $TiO_2$/$CsSnI_3$/P3HT/Au | 0.450 | 24.85 | 67.0 | 7.50 |
| **$CsSnI_3$ in this work** | FTO/compact $TiO_2$/mesoporous $TiO_2$/$CsSnI_3$/$Al_2O_3$/NiO/carbon | 0.520 | 23.40 | 66.0 | 8.03 |

## References

[1] X. Xu, Z. Liu, Z. Zuo, M. Zhang, Z. Zhao, Y. Shen, H. Zhou, Q. Chen, Y. Yang and M. Wang, *Nano Lett.*, 2015, **15**, 2402-2408.

[2] M. Kumar, S. Dharani, W. Leong, P. Boix, R. Prabhakar, T. Baikie, C. Shi, H. Ding, R. Ramesh, M. Asta, M. Graetzel, S. Mhaisalkar and N. Mathews, *Adv. Mater.*, 2014, **26**, 7122-7127.

[3] K. Marshall, R. Walton and R. Hatton, *J. Mater. Chem. A*, 2015, **3**, 11631-11640.

[4] K. Marshall, M. Walker, R. Walton and R. Hatton, *Nat Energy*, 2016, **1**, 1-9.

[5] T. Song, T. Yokoyama, S. Aramaki and M. Kanatzidis, *ACS Energy Lett.*, 2017, **2**, 897-903.

[6] J. Heo, J. Kim, H. Kim, S. Moon, S. Im and K. Hong, *J. Phys. Chem. Lett.*, 2018, **9**, 6024-6031.

[7] Y. Wang, J. Tu, T. Li, C. Tao, X. Deng and Z. Li, *J. Mater. Chem. A*, 2019, **7**, 7683-7690.

[8] T. Ye, K. Wang, Y. Hou, D. Yang, N. Smith, B. Magill, J. Yoon, R. Mudiyanselage, G. Khodaparast, K. Wang and S. Priya, *J. Am. Chem. Soc.*, 2021, **143**, 4319-4328.